Nitrogen atoms absolute density measurement using two-photon absorption laser induced fluorescence in reactive magnetron discharge for gallium nitride deposition

Lakshman Srinivasan, Laurent Invernizzi, Swaminathan Prasanna, Kristaq Gazeli, Nicolas Fagnon, Pere Roca i Cabarrocas, Guillaume Lombardi, Karim Ouaras

Nitrogen atoms absolute density measurement using Two-photon Absorption Laser Induced Fluorescence in reactive magnetron discharge for gallium nitride deposition

Lakshman Srinivasan[1,2], Laurent Invernizzi[3], Swaminathan Prasanna[3], Kristaq Gazeli[3], Nicolas Fagnon[3], Pere Roca i Cabarrocas[1,2], Guillaume Lombardi[3], Karim Ouaras[1,a)]

AFFILIATIONS

[1] LPICM - CNRS, Ecole Polytechnique, Institut Polytechnique de Paris, Palaiseau 91128, France.
[2] IPVF, Institut Photovoltaïque d'Ile-de-France, 18 Bd Thomas Gobert, 91120 Palaiseau, France.
[3] LSPM - CNRS, Université Sorbonne Paris Nord, 99 Av. J. B. Clément, 93430 Villetaneuse, France.

[a)] Author to whom correspondence should be addressed: karim.ouaras@polytechnique.edu

ABSTRACT

Low pressure-plasmas, in particular magnetron sputtering discharges, are increasingly used for the deposition of wide band gap semiconductor nitrides films (e.g. GaN or AlN) considering many benefits they exhibit with respect to conventional CVD techniques. Plasma-based solutions enable the dissociation of N_2 molecules into N-atoms under conditions that would not be possible with thermal process. However, as the dissociation rate remains quite small due to the strong nitrogen triple bond, it is somewhat complicated to determine and correlate the N-atoms density in the gas phase with that of the grown film in low-pressure discharges. Therefore, ns-TALIF has been carried out to determine the absolute density of N-atoms as a function of the pressure (tens of Pa range) in a Radio-Frequency sputtering plasma reactor used for GaN deposition. The TALIF set up has been optimized using a monochromator and adequate signal processing to enhance the detection limit, enabling the measurement of N-atoms density as low as 10^{11} cm^{-3} at 15 Pa. These measurements have been completed with electron density measurements performed in the same pressure range using microwave interferometry, thus providing quantitative data on both electron and N-atom densities that can be used for fundamental understanding, process optimization, and modeling of magnetron discharge intended for nitride semiconductor deposition.

Nitrogen-based plasmas are widely employed to produce or functionalize thin films that can address various industrial applications encompassing microelectronics[1], photonics[2], opto-electronics[3], photodetectors[4], telecommunications[5], photovoltaics[6], energy storage[7], sensors[8] and so on. Recently, a particular type of nitrides, namely GaN and AlN, respectively belonging to the family of wide and ultra-wide bandgap semiconductors (both spanning from ~2 up to ~6 eV), have drawn a lot of attention from the scientific community as they became necessary materials for devices that have to withstand higher voltages, frequencies and temperature compared to Silicon[9].

Such nitrides are produced through various technics including molecular beam epitaxy (MBE) and metal organic chemical vapor deposition (MOCVD). Nevertheless, these processes suffer from the drawbacks of operating at high temperature (> 800 °C) or making use of toxic precursor gases in large quantities. This makes these processes expensive and not environmentally friendly. Therefore, reactive sputtering has been considered as a good candidate for nitrides as it is more convenient than the abovementioned processes in the sense that it operates at a much lower temperature (as low as room temperature) and does not require toxic gas precursors (e.g. TMGa ($Ga(CH_3)_3$) or NH_3). Indeed, it simply requires a target made of the material of interest (e.g. Ga or Al) reacting with a plasma producing N-atoms trough N_2 dissociation. Several groups have demonstrated the growth of both materials using reactive sputtering[10–17]. In our previous work, we demonstrated that textured (c-axis) polycrystalline GaN thin films can be obtained using RF reactive magnetron sputtering under Ar/N_2 atmosphere at room temperature with growth rate as high a 3 $Å.s^{-1}$ [18]. We showed that the working pressure had the most influential impact on the structural quality of the films. Under our conditions, we notably found that pressure values up to 20 Pa enable to produce high quality films, which was somewhat unusual, as sputtering processes are known to be efficient under very low-pressure regime (i.e. a few Pa). These results have led us to question the fundamental aspects driving the synthesis of GaN films that exhibit such quality while working at room temperature. Moreover, regarding the high demand on such nitride materials and the potential of sputtering processes in providing a low-cost and greener solution for their widespread production, implementing plasma diagnostics for both process optimization and fundamental understanding is highly required. In particular, the determination of the absolute density of nitrogen in magnetron sputtering discharges may be of importance from several perspectives as it can help to: (i) determine the flux of particles reaching the substrate; (ii) adjust the stoichiometry of the film, (iii) optimize the growth rate; (iv) compare different sputtering systems based on absolute data and (v) discharge modeling as a useful input data.

However, it is well known that the dissociation of N_2 molecules to generate atomic nitrogen species in a plasma is a tough task to achieve due to the strong N≡N bond. Therefore, most of the time, N_2 is mixed with argon to enhance its dissociation[19,20].For instance, Tabbal *et al.* have measured a dissociation degree of 2.5% at a pressure of 7.5 Torr with Ar mixing ratio of 95% in a surface-wave-sustained plasma[21]. Many authors have characterized N_2 plasmas using several methods such as calibrated OES[22], OES actinometry[19], NO titration[23], VUV-absorption[24] or TALIF[25,26]. However, these were mainly conducted in plasma discharges working under moderate- to high-pressure regimes (from hundreds of Pa to atmospheric pressure) such as inductively couple plasma (ICP)[27] or micro-hollow cathode discharges[28]. As far as magnetron sputtering discharges are concerned, only a few studies are dealing with N-atoms density determination especially when considering the restriction on detection limit inherent to the low-pressure conditions. Even if TALIF seems to be well adapted to low-pressure plasmas since collisional quenching of excited states that prevails at high pressures can be discarded, the major drawback at lower pressures is that the strong background emission from N_2 FPS

overlaps with weaker fluorescence signal due to lower density of N-atoms and thus making the measurement of the N-atoms absolute density challenging.

In this paper, we use nanosecond (ns)-TALIF to probe N-atoms in a low-pressure plasma. The detection limit of the diagnostic is determined and noticeably enhanced by using a monochromator and adequate signal processing. This approach enables to detect N-atoms densities as low as 10^{11} cm^{-3}. These experiments have been carried out in a sputtering plasma reactor used for GaN deposition under Ar/N_2 environment. The main goal of this study is to provide quantitative data that can be used for fundamental understanding, process optimization, and modeling of magnetron discharges intended for nitride semiconductor deposition.

Figure 1 shows (a) the schematic representation of the reactor, the laser generation system and the light detection apparatuses used for TALIF experiments and (b) the two-photon excitation and fluorescence schemes of N- and Kr-atoms adopted in the present study. Experiments were carried out in a RF magnetron-sputtering reactor under deposition conditions used for polycrystalline GaN thin films[18]. The plasma was ignited thanks to a 2"-circular magnetron sputtering source (Torus® - Kurt J. Lesker Company) that houses a liquid gallium target. In this sputtering process, Ar and N_2 gases (99.9999% purity) were used to maximize the ejection of Ga-atoms from the target and to produce N-atom precursors in the gas phase, respectively. The magnetron was powered by a 300 W – RF generator (13.56 MHz) connected to an impedance matching box (TRUMPF PFG 300RF - Huttinger Elektronik). The system achieved a base vacuum pressure of about 10^{-5} Pa through a dry (nXDS-10iR scroll Pump) and a turbo-molecular pump (Alcatel ATP-900). This study focuses on determining the N-atoms absolute density as a function of the working gas pressure (from 2 to 32 Pa). In parallel, we performed microwave interferometry (MiWitron 2650 - f= 26.5 GHz) to determine the electron density using the same system and procedure described in the work of Ouaras et *al.*[29]. This was done to assess the correlation between the variation trend of N-atoms density and that of electrons as a function of the pressure. We chose the pressure as the varying parameter for two reasons: (i) it is the most influential parameter affecting the GaN crystalline quality in our experiments[18], and (ii) its variation allowed us to interrogate the TALIF measurement capacity by determining the detection threshold of N-atoms under low-density regime. For all TALIF experiments, the other plasma operating conditions were kept constant, namely a total gas flow of 20 sccm, an Ar/N_2 flow ratio of 5:2 and a RF power of 100 W.

For the determination of the N-atoms density, we performed ns-TALIF measurements. We used a tunable dye laser (Cobra-Stretch - Sirah Lasertechnik) pumped by the second harmonic of a 500 $mJ.pulse^{-1}$ Nd:YAG laser at 10 Hz that provides a pulse with a width of 10 ns (Quanta-Ray Lab-Series170-10 - Spectra-Physics). The dye laser beam was processed by two Beta Barium Borate (BBO) crystals, which yielded a laser beam with three harmonics separated using two fused silica Pellin-Broca prisms. We selected the desired third harmonic that was tuned in the regions of interest, i.e., 204 and 207 nm for Kr (204.221 nm) and N (206.767 nm) atoms, respectively. A typical energy value obtained for this harmonic is about 0.2 $mJ.pulse^{-1}$. The obtained pure UV-C radiation, that entered the reactor through a UV-fused silica window 2 cm above the cathode, was focused in order to have a beam diameter of 500 µm in the center of the reactor thanks to a lens with a 750 mm focal length (Figure 1.a). Subsequently, the laser beam exits the reactor through a second UV-fused silica window. Its diameter was adjusted using a 50 mm focal length lens to illuminate the calorimeter sensor (J-10MB-LE - Coherent) connected to an oscilloscope (TDS 3052, 500 MHz, 5 GS s^{-1} - Tektronix) that was placed at the laser line's end, ensuring continuous measurement of the laser's energy. To determine the absolute density of N-atoms, we used the same experimental procedure as that thoroughly described in the work of E. Bisceglia *et al.*[30]. The only difference with their work is that the fluorescence collection system was modified here by adding a monochromator (Model SP-2155, Princeton Instruments) before the fluorescence detector (photomultiplier tube, PMT - Hamamatsu, H11526-20-NF). This was necessary to better isolate the fluorescence lines and get rid as much as possible of the background plasma emission (notably from N_2 (FPS)) that strongly competes with the weak TALIF signal. Additionally, bandpass filters corresponding to N-atoms (Semrock FF02-740/13-25) and Kr-atoms (Semrock FF02-586/15-25) fluorescence wavelengths were placed in front of the entrance slit of the monochromator to block any stray light. Finally, different combinations of neutral density filters were used: (i) to properly adjust the laser energy and verify the quadratic dependence of the TALIF signal on the laser energy, and (ii) select the right laser energy to perform TALIF experiments (Figure 2). We should mention that all the TALIF measurements were averaged over 250 laser shots for each wavelength.

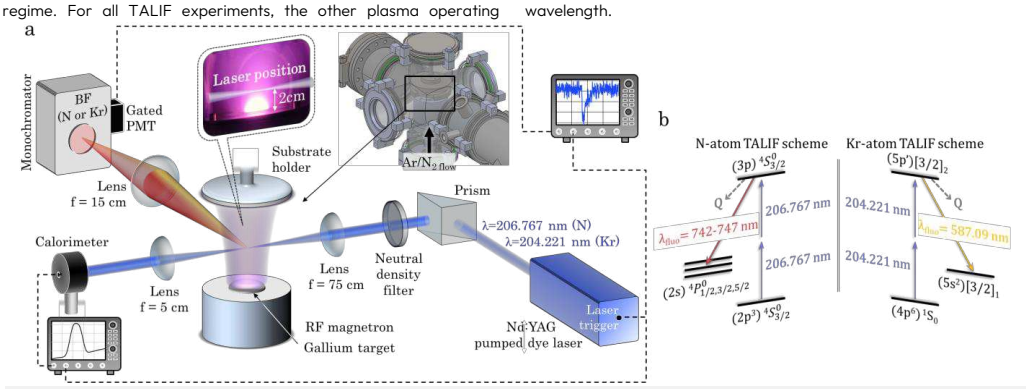

Figure 1. Scheme of the ns-TALIF experimental set-up (a) and two-photon excitation and fluorescence scheme of N- and Kr- atoms (b).

To determine the absolute densities of nitrogen from the collected fluorescence signals, a calibration procedure was performed using krypton gas. To this end, the reactor was first pumped down to 10^{-5} Pa for several hours to remove any impurities that could obscure the fluorescence measurement. Then, the reactor was filled with Krypton at a constant pressure of 100 Pa. An example of the Kr fluorescence temporal signal at the resonance wavelength (204.221 nm) at a laser energy of 77 µJ is shown in Figure 2.a_1. In this example, the effective lifetime of the laser-excited state of Kr is 29.5 ns, which is close to its natural lifetime, i.e. around 34 ns [4,5].The temporal integral of the TALIF signal at each wavelength around the resonance was then performed to retrieve the absorption profile at a given laser energy (Figure 2.a_2). The experimental absorption profile was well fitted by a Gaussian function, and was dominated by laser line width with negligible contribution from Doppler broadening of N-atom. The spectrally-integrated Gaussian profile was then plotted as a function of the square of the laser energy (Figure 2.a_3). A slope of a value of 1 must be retrieved if the double integral of the TALIF signal is proportional to the square of the laser energy. This condition is known as the "quadratic regime" and allows us to check the validity of the TALIF formula used for the calculation of the N-atoms density under our experimental conditions. In fact, besides the fluorescence and non-radiative decay (collisional quenching), no other effects should be involved in the depletion of the laser-excited state (e.g. photoionization or amplified stimulated emission). In this work, a slope of 0.99 was obtained with good accuracy, which satisfies the abovementioned condition (Figure 2.a_3). The same procedure was carried out for N-atoms to capture the corresponding temporally- and spectrally-integrated TALIF signals by appropriately selecting the laser energy. Figure 2.b_1 depicts a typical fluorescence signal of nitrogen at resonance (206.767 nm) for a laser energy of 262 µJ, obtained at a pressure of 26 Pa. Regarding the low-pressure conditions under which plasma experiments were performed, the signal-to-noise ratio (SNR) in this case is lower than in the case of Kr as the generated nitrogen density was close to the TALIF detection limit.

The effective lifetime of laser-excited N-atoms (27.1 ns) was extracted from this signal through an exponential fitting of its decaying part. The temporal integral of the signal at several wavelengths around the resonance follows a Gaussian profile (Figure 2.b_2) as in the case of Kr. The utility of the Gaussian fit is clearly justified here: as the nitrogen TALIF signal is weak, the Gaussian fitting allows for smoothing the profile to be obtained and used for spectral integration. The plot of the spectral integral of the Gaussian as a function of the square of the laser energy, allows verifying the necessary condition of having a slope of 1 (Figure 2.b_3). To maximize the SNR of the fluorescence signal in the case of N-atoms, the highest laser energy within the quadratic regime was chosen (dotted circle in Figure 2.b_3). A key factor for the determination of the N-atoms density is the natural lifetime $\tau_{nat\,(N^*)}$ of the fluorescing state of nitrogen. To determine it, the Stern-Volmer plot[31] was used (Figure 2.b_4). To apply this method, the pressure of N_2 in the chamber was varied between 14 and 33 Pa. The selection of this pressure range was dictated by the operating limits of the plasma and the SNR of the TALIF signal. Then, the inverse of the effective lifetime of the laser-excited state of N was plotted against the gas pressure, and the data were fitted with a linear function. Finally, by extrapolating the fitted line to zero pressure $\tau_{nat\,(N^*)}$ was found to be 27.3 +/- 1.5 ns. This value is in agreement with the relevant literature[32-34]. For the performance of the TALIF studies under the plasma conditions of the present study, the peak method was employed, which considers only one wavelength corresponding of the peak resonance of the fluorescence line[30]. Bisceglia *et al.* have demonstrated that the N-atoms densities determined by the peak method and the full profile method were in perfect agreement. This method allows reducing the time of recording of the TALIF data by avoiding capturing the entire absorption profile for each plasma condition. Since the line profile is Gaussian, the standard TALIF equation was modified by adding the contribution of the full width at half maximum (FWHM) of the line profile, which was only recorded for some representative conditions[30,35].

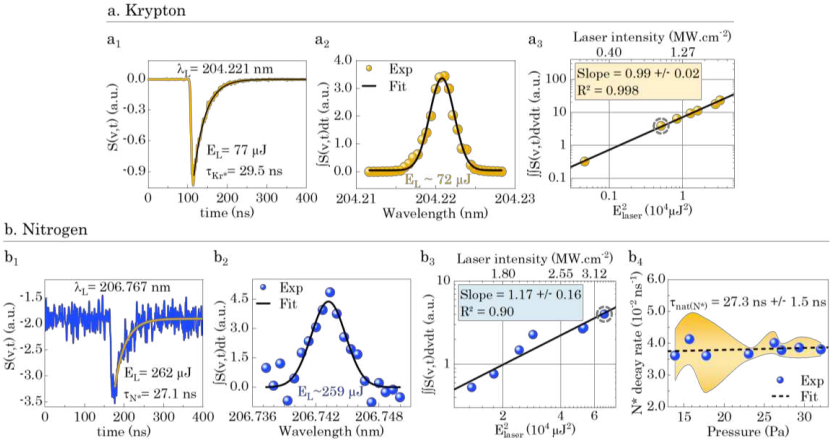

Figure 2. **a**.Krypton: example of a raw fluorescence signal obtained at resonance (a_1), temporally integrated signal measured at several wavelengths around resonance then fitted by a Gaussian (a_2), determination of the quadratic regime after temporal and spectral integration of fluorescence profiles for several laser energies (a_3). **b**. Nitrogen: example of raw fluorescence signal obtained at resonance (b_1), temporally integrated signal measured at several wavelengths around resonance, then fitted by a Gaussian (b_2), determination of the quadratic regime after temporal and spectral integration of fluorescence profiles for several laser energies (b_3), Stern-Volmer plot to determine the natural lifetime of N (b_4).

Therefore, we used equation (1) for the N-atoms density measurement via TALIF corresponding to the peak method[36]. In equation (1), n_X is the density of a species X (X here refers to N or Kr), $\int_t S_{F_{peak(X)}}$ the temporally integrated fluorescence signal of X, η_X the quantum efficiency of the detector at the fluorescence wavelength of X, T_X the transmission of the optics at the fluorescence wavelength of X, σ_X the two-photon excitation cross section of X, A_X the Einstein coefficient of the transition from the laser-excited level to a lower state of X, τ_X the experimentally-measured fluorescence decay time of the laser-excited state of X, E_X the laser energy selected for probing X atom, λ_X the laser wavelength chosen to perform TALIF measurements at the center of the absorption line of X, and $g_{\nu_{peak(X)}}$ the measured two-photon absorption profile of X. In equation (1), the ratio $g_{\nu_{peak(Kr)}}/g_{\nu_{peak(N)}}$ corresponds to the inversed ratio of the FWHM, $FWHM_{(N)}/FWHM_{(Kr)}$[32]. The values of the parameters of the equation (1) are listed in Table 1.

$$n_N = n_{Kr}\frac{\int_t S_{F_{peak(N)}}}{\int_t S_{F_{peak(Kr)}}}\frac{\eta_{Kr}}{\eta_N}\frac{T_{Kr}}{T_N}\frac{\sigma_{Kr}}{\sigma_N}\frac{A_{Kr}}{A_N}\frac{\tau_{Kr}}{\tau_N}\frac{E_{Kr}{}^2}{E_N{}^2}\frac{\lambda_{Kr}{}^2}{\lambda_N{}^2}\frac{g_{\nu_{peak(Kr)}}}{g_{\nu_{peak(N)}}} \quad (1)$$

In the following, the systematic error associated with each determined N-atoms density will not be shown as it is close to 60%, mainly due to the 50% uncertainty of the value of the two-photon absorption cross section ratio[37]. Therefore, only the average values are displayed along with the statistical error obtained by calculating the standard deviation from three independent measurements. Figure 3.a presents the density variation of N-atoms as a function of the N_2 pressure in the reactor. As a reminder, these experiments were conducted in Ar/N_2 (5:2 ratio) at a total gas flow of 20 sccm using 100 W of RF power. All the measurement points in Figure 3.a are accompanied by their corresponding peak fluorescence profiles obtained at resonance as represented in Figure 3.a'. TALIF measurements of N-atoms for pressures below 15 Pa were not possible as the SNR ratio became too small to distinguish the fluorescence signal from noise. Based on our estimations, using the current ns-TALIF set-up, the detection limit of N-atoms is around 10^{11} cm^{-3}. In Figure 3.a, we observe a progressive increase of the N-atoms density from 4×10^{11} to 1.4×10^{12} cm^{-3} by varying the pressure from 16 Pa to 32 Pa, respectively. Within the investigated pressure range, the N-atoms density increases by a factor of 3.25 while the pressure increases by a factor of 2. It is noteworthy that the operation of such plasma source at pressures as high as 30 Pa may be beneficial for applications in which the strong production of N-atoms is desirable. For instance, this would represent a way to increase the growth rate of nitride-based coatings or to improve the efficiency of nitridation processes while working at relatively low pressure that ensures low-level of contamination.

A possible cause leading to the increase of the N-atoms density as a function of the pressure may be the enhancement of the electron density, which induces a larger dissociation degree of N_2 through direct (i.e., $e^- + N_2 \rightarrow N + N$) or indirect mechanisms, e.g., through electron collisions with vibrationally excited N_2 molecules[27]. Our measurements indicate a similar variation trend of the electron density n_e with that of the N-atoms density (Figure 3.b) except that the electron density is doubled between 16 Pa and 32 Pa, i.e., from 0.5×10^{11} cm^{-3} to 1×10^{11} cm^{-3}, respectively, while N-atoms density increases by a factor of 3.25. Therefore, while the enhancement of the production of N-atoms is likely to be attributed to the increase of the electron density, it seems that other processes may also enter into play. For instance, one may think about reactions that involved Argon ions and N_2 molecules trough charge exchange reactions ($Ar^+ + N_2 \rightarrow Ar + N_2^+$) followed by dissociative recombination ($e^- + N_2^+ \rightarrow N + N$) or that would be the consequence of reactions of Ar metastable with N_2[19]. This hypothesis has to be taken cautiously considering the uncertainty in the N-atoms density measurements described earlier. In the following studies of ours, further experiments will be carried out to determine the Ar metastable density as well as to model the discharge for shedding more light on the key reactions that drive the N-atoms production in such discharge.

In this letter, we have established the application's domain of ns-TALIF for N-atoms density measurements in a RF magnetron discharge under conditions of GaN deposition. As this work is intended to provide quantitative data for plasma modeling and fundamental research, we also determined the electron density simultaneously with the TALIF measurements. Notably, we have observed that in the range of low pressures investigated here (16 to 32 Pa), which are higher than those used in conventional sputtering systems, the N-atoms density increased by a factor of 3.25 while the electron density exhibited a two-fold increment within this pressure range. This would suggest that the production of N-atoms is not only driven by electrons but other mechanisms as well such as charge exchange reactions between Ar^+ and N_2, dissociative recombination of e^- and N_2^+ or energy exchanges between Ar metastables and N_2. This enhancement of N-atoms production when working at such low-pressure range would be beneficial for applications that target high growth rates.

This work was funded by the French National Research Agency trough contract No. ANR-22-CE51-0011-01 (GASPE project), No. ANR-IEED-002-01 and ANR-20-CE51-0020 (ULTRAMAP project); and the Île-de-France region (project SESAME DIAGPLAS). Authors would like to thank the MITI-CNRS - "Réseau des Plasmas Froids" for providing the MWI. We are grateful to Marc Malvaux, Cédric Noël and Ludovic William for their help with the reactor's transportation, MWI installation and experimental installation, respectively.

Parameter	$\int_t S_{F_{peak(X)}}$		η_X		T_X		$\frac{\sigma_{Kr}}{\sigma_N}$	A_X		τ_X		E_X		λ_X		$g_{\nu_{peak(X)}}$	
Unit	a.u.		no unit		no unit		no unit	s^{-1}		ns		µJ		nm		s	
X species	Kr	N	Kr	N	Kr	N	NA	Kr	N	Kr	N	Kr	N	Kr	N	Kr	N
Value	7.96×10^{-9}	Variable	0.468	0.4836	0.92	0.92	0.62	1.17×10^{6}	3.38×10^{6}	28.7	Pressure dependent	≈127	≈259	204.221	206.767	6.28×10^{-12}	7.12×10^{-12}
Uncertainty (%)	10	10	10	10	5	5	50	6	12	10	10	8	8	None	None	14	16
Reference	Meas.		Manuf.		Manuf.		Niemi *et al.*[32]	Niemi *et al.*[32]	Meas.	Meas.		Meas.		Meas.		Meas.	Meas.

Table 1. Detailed list of the parameters used for N-atoms determination. *"Meas." and "Manuf." stand for experimentally measured and manufacturer data, respectively.*

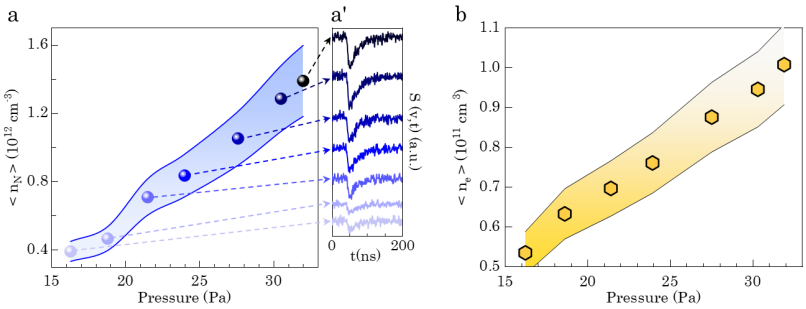

Figure 3. Atomic density of nitrogen as a function of pressure (a), associated with fluorescence profiles obtained at resonance (a') and electron density as a function of pressure (b).

AUTHOR DECLARATIONS

Conflict of Interest

The authors have no conflicts to disclose.

Author Contributions

Lakshman Srinivasan: Investigation (lead); Formal analysis (supporting); Conceptualization (equal); Visualization (supporting); Writing – review & editing (equal). **Laurent Invernizzi:** Investigation (equal); Methodology (equal); Formal analysis (equal); Writing – original draft (equal); Writing – review & editing (equal). **Swaminathan Prasanna:** Supervision (equal); Formal analysis (equal); Methodology (supporting); Writing – review & editing (equal). **Kristaq Gazeli:** Writing – original draft (equal); Writing – review & editing (equal). **Nicolas Fagnon:** Investigation (supporting); Writing – review & editing (equal). **Pere Roca i Cabarrocas:** Writing – review & editing (equal). **Guillaume Lombardi:** Supervision (equal); Funding acquisition (equal); Project administration (equal); Writing – review & editing (equal). **Karim Ouaras:** Supervision (equal); Conceptualization (equal); Funding acquisition (equal); Investigation (equal); Methodology (equal); Project administration (equal); Visualization (equal); Writing – original draft (lead); Writing – review & editing (equal).

Data availability

The data that support the findings of this study are available from the corresponding authors upon reasonable request.

REFERENCES

(1) Zhong, Y.; Zhang, J.; Wu, S.; Jia, L.; Yang, X.; Liu, Y.; Zhang, Y.; Sun, Q. A Review on the GaN-on-Si Power Electronic Devices. *Fundam. Res.* **2022**, *2* (3), 462–475. https://doi.org/10.1016/j.fmre.2021.11.028.

(2) Li, N.; Ho, C. P.; Zhu, S.; Fu, Y. H.; Zhu, Y.; Lee, L. Y. T. Aluminium Nitride Integrated Photonics: A Review. *Nanophotonics* **2021**, *10* (9), 2347–2387. https://doi.org/doi:10.1515/nanoph-2021-0130.

(3) van Deurzen, L.; Nguyen, T.-S.; Casamento, J.; Xing, H. G.; Jena, D. Epitaxial Lattice-Matched AlScN/GaN Distributed Bragg Reflectors. *Appl. Phys. Lett.* **2023**, *123* (24), 241104. https://doi.org/10.1063/5.0176707.

(4) Fan, Z.; Qin, Z.; Jin, L.; Yue, Z.; Li, B.; Zhang, W.; Wang, Y.; Wu, H.; Sun, Z. A Solar-Blind Vacuum-Ultraviolet Photodetector Based on Free-Standing Lamellar Aluminum Nitride Single Crystal. *Appl. Phys. Lett.* **2023**, *123* (23), 232104. https://doi.org/10.1063/5.0172734.

(5) Zhang, C.; Tran, M. A.; Zhang, Z.; Dorche, A. E.; Shen, Y.; Shen, B.; Asawa, K.; Kim, G.; Kim, N.; Levinson, F.; Bowers, J. E.; Komljenovic, T. Integrated Photonics beyond Communications. *Appl. Phys. Lett.* **2023**, *123* (23), 230501. https://doi.org/10.1063/5.0184677.

(6) Wei, H.; Wu, J.; Qiu, P.; Liu, S.; He, Y.; Peng, M.; Li, D.; Meng, Q.; Zaera, F.; Zheng, X. Plasma-Enhanced Atomic-Layer-Deposited Gallium Nitride as an Electron Transport Layer for Planar Perovskite Solar Cells. *J Mater Chem A* **2019**, *7*(44), 25347–25354. https://doi.org/10.1039/C9TA08929B.

(7) Moradpour, M.; Ghani, P.; Gatto, G. A GaN-Based Battery Energy Storage System for Residential Application. In *2019 International Conference on Clean Electrical Power (ICCEP)*; 2019; pp 427–432. https://doi.org/10.1109/ICCEP.2019.8890238.

(8) Polster, T.; Hoffmann, M. Aluminum Nitride Based 3D, Piezoelectric, Tactile Sensor. *Procedia Chem.* **2009**, *1* (1), 144–147. https://doi.org/10.1016/j.proche.2009.07.036.

(9) Bader, S. J.; Lee, H.; Chaudhuri, R.; Huang, S.; Hickman, A.; Molnar, A.; Xing, H. G.; Jena, D.; Then, H. W.; Chowdhury, N.; Palacios, T. Prospects for Wide Bandgap and Ultrawide Bandgap CMOS Devices. *IEEE Trans. Electron Devices* **2020**, *67* (10), 4010–4020. https://doi.org/10.1109/TED.2020.3010471.

(10) Ross, J.; Rubin, M. High-Quality GaN Grown by Reactive Sputtering. *Mater. Lett.* **1991**, *12*(4), 215–218. https://doi.org/10.1016/0167-577X(91)90001-M.

(11) Monish, M.; Mohan, S.; Sutar, D. S.; Major, S. S. Gallium Nitride Films of High N-Type Conductivity Grown by Reactive Sputtering. *Semicond. Sci. Technol.* **2020**, *35*(4), 045011. https://doi.org/10.1088/1361-6641/ab73ec.

(12) Dimitrova, V.; Manova, D.; Paskova, T.; Uzunov, Tz.; Ivanov, N.; Dechev, D. Aluminium Nitride Thin Films Deposited by DC Reactive Magnetron sputteringfn2fn2Paper Presented at the 10th International School on Vacuum Electron and Ion Technologies, 22–27 September 1997, Varna, Bulgaria. *Vacuum* **1998**, *51* (2), 161–164. https://doi.org/10.1016/S0042-207X(98)00150-X.

(13) Liu, W.; Xu, W.; Wang, W.; He, L.; Zhou, J.; Radhakrishnan, K.; Yu, H.; Ren, J. RF Reactive Sputtering AlN Thin Film at Room Temperature for CMOS-Compatible MEMS Application. In *2017 Joint IEEE International Symposium on the Applications of Ferroelectric (ISAF)/International Workshop on Acoustic Transduction Materials and Devices (IWATMD)/Piezoresponse Force Microscopy (PFM)*; 2017; pp 52–55. https://doi.org/10.1109/ISAF.2017.8000210.

(14) Prabaswara, A.; Birch, J.; Junaid, M.; Serban, E. A.; Hultman, L.; Hsiao, C.-L. Review of GaN Thin Film and Nanorod Growth Using Magnetron Sputter Epitaxy. *Appl. Sci.* **2020**, *10*(9). https://doi.org/10.3390/app10093050.

(15) Morikawa, S.; Ueno, K.; Kobayashi, A.; Fujioka, H. Pulsed Sputtering Preparation of InGaN Multi-Color Cascaded LED Stacks for Large-Area Monolithic Integration of RGB LED Pixels. *Crystals* **2022**, *12* (4). https://doi.org/10.3390/cryst12040499.

(16) Watanabe, T.; Ohta, J.; Kondo, T.; Ohashi, M.; Ueno, K.; Kobayashi, A.; Fujioka, H. AlGaN/GaN Heterostructure Prepared on a Si (110) Substrate via Pulsed Sputtering. *Appl. Phys. Lett.* **2014**, *104* (18), 182111. https://doi.org/10.1063/1.4876449.

(17) Maeda, R.; Ueno, K.; Kobayashi, A.; Fujioka, H. AlN/Al0.5Ga0.5N HEMTs with Heavily Si-Doped Degenerate GaN Contacts Prepared via Pulsed Sputtering. *Appl. Phys. Express* **2022**, *15* (3), 031002. https://doi.org/10.35848/1882-0786/ac4fcf.

(18) Srinivasan, L.; Jadaud, C.; Silva, F.; Vanel, J.-C.; Maurice, J.-L.; Johnson, E.; Roca i Cabarrocas, P.; Ouaras, K. Reactive Plasma Sputtering Deposition of Polycrystalline GaN Thin Films on Silicon Substrates at Room Temperature. *J. Vac. Sci. Technol. A* **2023**, *41* (5), 053407. https://doi.org/10.1116/6.0002718.

(19) Czerwiec, T.; Greer, F.; Graves, D. B. Nitrogen Dissociation in a Low Pressure Cylindrical ICP Discharge Studied by Actinometry and Mass Spectrometry. *J. Phys. Appl. Phys.* **2005**, *38* (24), 4278. https://doi.org/10.1088/0022-3727/38/24/003.

(20) Kang, N.; Gaboriau, F.; Oh, S.; Ricard, A. Modeling and Experimental Study of Molecular Nitrogen Dissociation in an Ar–N2 ICP Discharge. *Plasma Sources Sci. Technol.* **2011**, *20* (4), 045015. https://doi.org/10.1088/0963-0252/20/4/045015.

(21) Tabbal, M.; Kazopoulo, M.; Christidis, T.; Isber, S. Enhancement of the Molecular Nitrogen Dissociation Levels by Argon Dilution in Surface-Wave-Sustained Plasmas. *Appl. Phys. Lett.* **2001**, *78* (15), 2131–2133. https://doi.org/10.1063/1.1359775.

(22) Salmon, A.; Popov, N. A.; Stancu, G. D.; Laux, C. O. Quenching Rate of N(2P) Atoms in a Nitrogen Afterglow at Atmospheric Pressure. *J. Phys. Appl. Phys.* **2018**, *51* (31), 314001. https://doi.org/10.1088/1361-6463/aace71.

(23) Vašina, P.; Kudrle, V.; Tálský, A.; Botoš, P.; Mrázková, M.; Meško, M. Simultaneous Measurement of N and O Densities in Plasma Afterglow by Means of NO Titration. *Plasma Sources Sci. Technol.* **2004**, *13* (4), 668. https://doi.org/10.1088/0963-0252/13/4/016.

(24) Remigy, A.; Kasri, S.; Darny, T.; Kabbara, H.; William, L.; Bauville, G.; Gazeli, K.; Pasquiers, S.; Sousa, J. S.; Oliveira, N. D.; Sadeghi, N.; Lombardi, G.; Lazzaroni, C. Cross-Comparison of Diagnostic and 0D Modeling of a Micro-Hollow Cathode Discharge in the Stationary Regime in an Ar/N2 Gas Mixture. *J. Phys. Appl. Phys.* **2021**, *55* (10), 105202. https://doi.org/10.1088/1361-6463/ac3c74.

(25) Adams, S. F.; Miller, T. A. Two-Photon Absorption Laser-Induced Fluorescence of Atomic Nitrogen by an Alternative Excitation Scheme. *Chem. Phys. Lett.* **1998**, *295* (4), 305–311. https://doi.org/10.1016/S0009-2614(98)00972-5.

(26) Chng, T. L.; Lepikhin, N. D.; Orel, I. S.; Popov, N. A.; Starikovskaia, S. M. TALIF Measurements of Atomic Nitrogen in the Afterglow of a Nanosecond Capillary Discharge. *Plasma Sources Sci. Technol.* **2020**, *29* (3), 035017. https://doi.org/10.1088/1361-6595/ab6f9c.

(27) Kimura, T.; Kasugai, H. Experiments and Global Model of Inductively Coupled Rf Ar/N2 Discharges. *J. Appl. Phys.* **2010**, *108* (3), 033305. https://doi.org/10.1063/1.3468603.

(28) Remigy, A.; Aubert, X.; Prasanna, S.; Gazeli, K.; Invernizzi, L.; Lombardi, G.; Lazzaroni, C. Absolute N-Atom Density Measurement in an Ar/N2 Micro-Hollow Cathode Discharge Jet by Means of Ns-Two-Photon Absorption Laser-Induced Fluorescence. *Phys. Plasmas* **2022**, *29* (11), 113508. https://doi.org/10.1063/5.0110318.

(29) Ouaras, K.; Lombardi, G.; Couëdel, L.; Arnas, C.; Hassouni, K. Microarcing-Enhanced Tungsten Nano and Micro-Particles Formation in Low Pressure High-Density Plasma. *Phys. Plasmas* **2019**, *26* (2), 023705. https://doi.org/10.1063/1.5083583.

(30) Bisceglia, E.; Prasanna, S.; Gazeli, K.; Aubert, X.; Duluard, C. Y.; Lombardi, G.; Hassouni, K. Investigation of N(4S) Kinetics during the Transients of a Strongly Emissive Pulsed ECR Plasma Using Ns-TALIF. *Plasma Sources Sci. Technol.* **2021**, *30* (9), 095001. https://doi.org/10.1088/1361-6595/ac0da1.

(31) Gazeli, K.; Aubert, X.; Prasanna, S.; Duluard, C. Y.; Lombardi, G.; Hassouni, K. Picosecond Two-Photon Absorption Laser-Induced Fluorescence (Ps-TALIF) in Krypton: The Role of Photoionization on the Density Depletion of the Fluorescing State Kr 5p'[3/2]2. *Phys. Plasmas* **2021**, *28* (4), 043301. https://doi.org/10.1063/5.0041471.

(32) Niemi, K.; Gathen, V. S. der; Döbele, H. F. Absolute Calibration of Atomic Density Measurements by Laser-Induced Fluorescence Spectroscopy with Two-Photon Excitation. *J. Phys. Appl. Phys.* **2001**, *34* (15), 2330. https://doi.org/10.1088/0022-3727/34/15/312.

(33) Schmidt, J. B.; Roy, S.; Kulatilaka, W. D.; Shkurenkov, I.; Adamovich, I. V.; Lempert, W. R.; Gord, J. R. Femtosecond, Two-Photon-Absorption, Laser-Induced-Fluorescence (Fs-TALIF) Imaging of Atomic Hydrogen and Oxygen in Non-Equilibrium Plasmas. *J. Phys. Appl. Phys.* **2016**, *50* (1), 015204. https://doi.org/10.1088/1361-6463/50/1/015204.

(34) Boogaarts, M. G. H.; Mazouffre, S.; Brinkman, G. J.; van der Heijden, H. W. P.; Vankan, P.; van der Mullen, J. A. M.; Schram, D. C.; Döbele, H. F. Quantitative Two-Photon Laser-Induced Fluorescence Measurements of Atomic Hydrogen Densities, Temperatures, and Velocities in an Expanding Thermal Plasma. *Rev. Sci. Instrum.* **2002**, *73* (1), 73–86. https://doi.org/10.1063/1.1425777.

(35) Stancu, G. D. Two-Photon Absorption Laser Induced Fluorescence: Rate and Density-Matrix Regimes for Plasma Diagnostics. *Plasma Sources Sci. Technol.* **2020**, *29* (5), 054001. https://doi.org/10.1088/1361-6595/ab85d0.

(36) Invernizzi, L.; Duluard, C. Y.; Höft, H.; Hassouni, K.; Lombardi, G.; Gazeli, K.; Prasanna, S. Peculiarities of Measuring Fluorescence Decay Times by a Streak Camera for Ps-TALIF Experiments in Reactive Plasmas. *Meas. Sci. Technol.* **2023**, *34* (9), 095203. https://doi.org/10.1088/1361-6501/acd8db.

(37) Gazeli, K.; Lombardi, G.; Aubert, X.; Duluard, C. Y.; Prasanna, S.; Hassouni, K. Progresses on the Use of Two-Photon Absorption Laser Induced Fluorescence (TALIF) Diagnostics for Measuring Absolute Atomic Densities in Plasmas and Flames. *Plasma* **2021**, *4* (1), 145–171. https://doi.org/10.3390/plasma4010009.